The 2019 World Congress on
Advances in Structural Engineering and Mechanics (ASEM19)
Jeju Island, Korea, September 17 - 21, 2019

Short beam-column tests of cold-formed steel semi-oval hollow sections

* Man-Tai Chen[1)] and Ben Young[2)]

[1)] *Department of Civil Engineering, The University of Hong Kong, Pokfulam Rd., Hong Kong, China.*
[2)] *Department of Civil and Environmental Engineering, The Hong Kong Polytechnic University, Hong Kong, China. (Formerly, Department of Civil Engineering, The University of Hong Kong, Pokfulam Rd., Hong Kong, China)*
[1)] *cmt111@connect.hku.hk*

ABSTRACT

Experimental investigation on cold-formed steel semi-oval hollow section short members under combined compression and uniaxial bending is presented. Four cross-section series were included. A total of 21 semi-oval hollow section beam-columns with specimen length of 440 mm were tested at various loading eccentricities in order to investigate the ultimate load-carrying capacities, the load-end rotation responses and the load-moment interaction relationship for each test series. The specimens in this study were compact sections. Although the design of cold-formed steel semi-oval sections is not explicitly included in the current design specifications, the experimental results were compared with the design predictions by the North American Specification (AISI S100) and the American Specification (AISC 360) using the interaction curves specified in these design specifications. The applicability of the current design rules for cold-formed steel semi-oval hollow sections short beam-column members was assessed. Generally, the predictions by the North American and American Specifications are quite conservative for cold-formed steel semi-oval hollow section short beam-columns under combined compression and uniaxial bending.

1. INTRODUCTION

The development of cold-forming technology has enabled the formation of various desirable cross-section shapes, such as elliptical section (Chen and Young 2019a, b, d), oval section, hexagonal section (Xu *et al.* 2016a, b), octagonal section (Chen *et al.* 2019, Ding *et al.* 2016, Fang *et al.* 2018, Zhu *et al.* 2019) and semi-oval hollow section (SOHS) in this study. Semi-oval hollow section consists of one semi-circular and three flat walls as shown in Fig. 1. The prominent structural efficiency and appealing

[1)] Post-Doctoral Fellow
[2)] Professor

architectural appearance of SOHS but yet limited investigations on such section have urged the need to study the structural performance of SOHS under various types of loading, such as in compression (Chen and Young 2018a, b) and bending (Chen and Young 2019c). However, there is no investigation on cold-formed steel SOHS beam-column members.

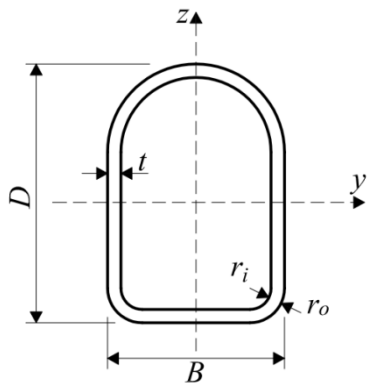

Fig. 1 Cross-sectional view of SOHS

This paper describes an experimental study on cold-formed steel compact SOHS short beam-columns under combined compression and uniaxial bending. The initial geometric imperfections of specimens were measured prior to the beam-column tests. The ultimate load-carrying capacities, load-end rotation responses as well as load-moment interaction relationships for SOHS short beam-columns are presented. Although the design of cold-formed steel semi-oval sections is not explicitly included in the current design specifications, the experimental results were compared with the design predictions by the North American Specification (AISI-S100 2016) and the American Specification (ANSI/AISC360 2016) using the interaction curves specified in these design specifications. The applicability of the current design rules for cold-formed steel compact SOHS short beam-column members was assessed.

2. TEST SPECIMENS

A total of 21 SOHS short beam-columns were tested. Four cross-section series of compact SOHS were included, which were cold-formed from the hot-extruded seamless steel circular hollow sections. Tensile coupon tests were conducted to obtain the material properties of SOHS. The material properties have been reported in Chen and Young (2018a) as the short beam-column specimens in this study were from the same batch of SOHS tubes as used in the stub column tests (Chen and Young 2018a). Fig. 1 shows the definition of symbols describing the cross-section geometry of SOHS. The nominal cross-section dimensions (D×B×t) of SOHS were 93×62×5.5, 107×68×6.5, 108×79×5.5 and 125×85×6.5, where D, B and t are the overall depth, overall width and wall thickness of the section, respectively. The specimens were machined to a

specified length (L) of 440 mm, then the specimen ends were flattened and welded onto 25.4 mm thick end plates.

The naming system of specimens included detailed information about the nominal cross-section geometry, specimen length and loading eccentricity. The letter SBC in the suffix of the specimen label indicates short beam-columns with specimen length of 440 mm. The letter 'e' and the following value indicate the targeted loading eccentricity (e) of the specimen. A symbol of "#" was used to denote the repeated test. For instance, the label 107×68×6.5-SBCe15 means a short beam-column with specimen length of 440 mm loaded at a targeted eccentricity of 15 mm with nominal cross-section dimensions (D×B×t) being 107×68×6.5. The measured values of loading eccentricities and specimen dimensions are tabulated in Table 1.

Table 1 Measured dimensions, loading eccentricities and initial global geometric imperfections of beam-column specimens

Specimen	D (mm)	B (mm)	t (mm)	r_o (mm)	r_i (mm)	$e+\omega_g$ (mm)	ω_g/L
93×62×5.5-SBCe5	93.3	62.0	5.1	14.7	9.6	4.23	0
93×62×5.5-SBCe12	93.4	62.0	5.3	15.8	10.5	11.75	0
93×62×5.5-SBCe25	93.4	62.0	5.3	15.7	10.3	23.48	1/1732
93×62×5.5-SBCe50	93.3	62.0	5.5	14.7	9.3	47.14	0
93×62×5.5-SBCe100	93.4	62.0	5.5	15.3	9.8	99.03	1/1732
107×68×6.5-SBCe8	107.4	68.0	6.3	15.7	9.3	6.80	0
107×68×6.5-SBCe15	107.4	67.8	6.6	15.9	9.3	12.68	1/1732
107×68×6.5-SBCe30	107.5	67.9	6.6	15.7	9.1	27.57	1/1732
107×68×6.5-SBCe60	107.2	68.0	6.4	14.6	8.2	59.69	0
107×68×6.5-SBCe110	107.3	67.9	6.3	14.5	8.2	107.51	0
108×79×5.5-SBCe9	108.4	79.1	5.6	12.8	7.3	8.09	1/3465
108×79×5.5-SBCe15	108.3	79.1	5.5	13.4	7.9	14.13	0
108×79×5.5-SBCe30	108.3	79.1	5.5	13.4	7.9	27.57	0
108×79×5.5-SBCe60	108.3	79.1	5.6	12.9	7.3	59.99	0
108×79×5.5-SBCe120	108.3	79.0	5.5	13.8	8.3	120.34	0
108×79×5.5-SBCe120#	108.2	79.0	5.4	12.3	6.9	119.70	1/693
125×85×6.5-SBCe8	124.9	85.1	6.4	16.5	10.0	6.77	0
125×85×6.5-SBCe15	124.8	85.2	6.4	15.9	9.6	13.85	0
125×85×6.5-SBCe30	124.9	85.1	6.5	16.9	10.4	31.07	0
125×85×6.5-SBCe60	124.8	85.1	6.4	17.0	10.6	57.92	0
125×85×6.5-SBCe90	124.8	85.0	6.3	16.7	10.3	88.66	0

3. INITIAL GEOMETRIC IMPERFECTION MEASUREMENTS

The initial global geometric imperfections (ω_g) of specimens were measured before the beam-column tests by a Leica TCR405 total-station using the same method as reported in Chen and Young (2018b). The global imperfection was assumed to be in

a bow shape and the sign convention is shown in Fig. 2. The measured initial global geometric imperfections at mid-length for each specimen were normalized to the specimen length as summarized in Table 1. The insignificant global imperfections for each series demonstrate the great straightness of the tubes.

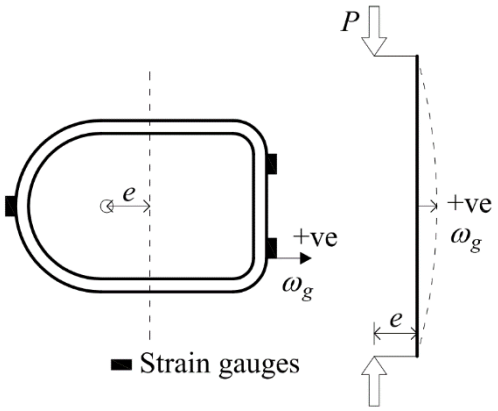

Fig. 2 Strain gauge arrangement and the sign convention of initial global geometric measurement

4. BEAM-COLUMN TESTS

4.1 Test setup and procedure

The SOHS short beam-columns were compressed between pinned ends with various loading eccentricities as shown in Fig. 3. Same special bearing system as described in Chen and Young (2018b) was adopted in this study to simulate the pin-ended conditions. The special bearing system was specially designed such that the beam-column specimens were free to rotate about the major axis, whilst the rotations about the orthogonal axis were restrained. The lower pit plate was mounted to a lockable sitting with the upper one affixed to the loading frame. The specimens were positioned at the targeted loading eccentricity and were then fastened to the wedge plates. Single curvature and uniform bending moment about the major axis in positive direction (semi-circular flange in compression) were attained along the specimens.

Three vertical LVDTs were installed to measure the axial shortening and end rotation of specimen. Another horizontal LVDT was installed at the mid-length of specimen on the tension side to measure the lateral deflection. Displacement-controlled loading method with a constant speed of 0.5 mm/min was used to apply compressive force to the specimens. The applied displacement was paused for 100 seconds near ultimate load to obtain the static responses of beam-columns. A data acquisition system was used to record the applied load, readings from LVDTs and strain gauges at 1 second intervals throughout the tests.

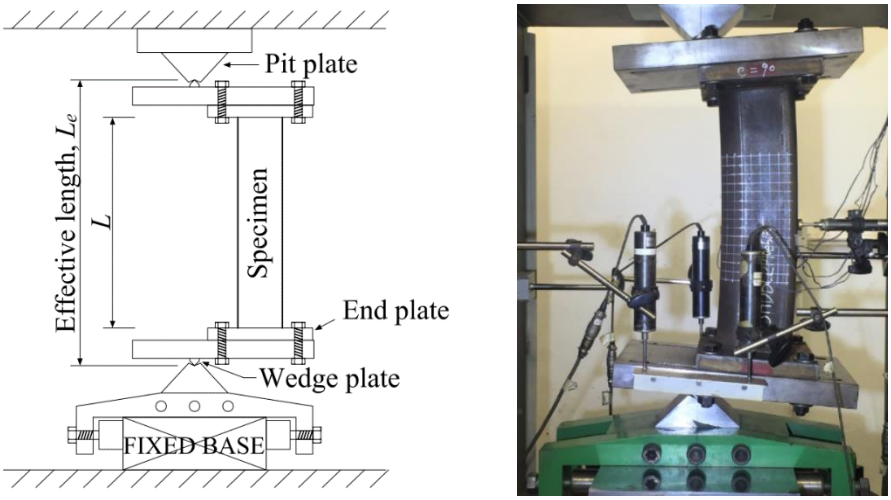

Fig. 3 Test setup and test rig for SOHS short beam-columns

4.1 Loading eccentricity

Before testing, the geometric center of SOHS for each specimen was calculated and marked. The specimen was initially positioned to the targeted loading eccentricity. The loading eccentricity was measured using a Leica TCR405 total-station by reading and converting the space coordinates of the centers of pit plates and the specimen. Three strain gauges were also adhered on the mostly stressed fibers as shown in Fig. 2. Based on the readings of strain gauges, the corresponding applied load and lateral deflection at mid-length, the loading eccentricity of beam-column can be determined. Within the elastic loading range, the bending moment of the specimen at mid-length can be expressed by Eqs. (1) and (2). By equating Eq. (1) with Eq. (2), the measured loading eccentricity obtained from strain gauge readings with the initial global imperfection can be obtained and expressed by Eq. (3). In this study, the measured loading eccentricities obtained from strain gauge readings were used up to 50 mm, beyond which the measured loading eccentricities obtained from the total-station were used. The measured loading eccentricities are reported in Table 1.

$$M = P\left(e + \omega_g + \Delta\right) \tag{1}$$

$$M = EI_y\kappa \tag{2}$$

$$\left(e + \omega_g\right) = EI_y\kappa / P - \Delta \tag{3}$$

where EI_y is the flexural rigidity of the cross-section about the bending axis, κ is the curvature of the specimen and is expressed as the strain gradient of the section under bending, P is the applied compressive load, e is the eccentricity at specimen ends, ω_g is the initial global geometric imperfection and Δ is the lateral deflection of specimen at mid-height in the bending direction.

4.2 Test results

The static experimental load-carrying capacities (P_{Exp}), the end moments at ultimate ($M_{end,Exp}$) and the second-order inelastic moments at mid-length of specimen at ultimate ($M_{mid,Exp}$) are tabulated in Tables 2-5. The effective length (L_e) of the beam-column was taken as the distance between the tips of upper and lower knife-edged wedges, and equaled to the sum of specimen length, the thicknesses of two end plates (50.8 mm) and the heights of two wedge plates (122.8 mm) as illustrated in Fig. 3. The end moment and second-order inelastic moment at mid-length of specimen corresponding to the ultimate applied axial load were obtained by Eqs. (4) and (5), respectively.

$$M_{end,Exp} = e\, P_{Exp} \tag{4}$$

$$M_{mid,Exp} = P_{Exp}\left(e + \omega_g + \Delta_u\right) \tag{5}$$

where Δ_u is the measured lateral deflection at mid-length of the specimen corresponding to the ultimate axial load.

All short beam-column specimens failed by material yielding since the SOHS in the test program were compact sections. The static load-end rotation responses and load-moment relationships for Series 93×62×5.5-SBC are depicted in Figs. 4 and 5.

Table 2 Test results and design strength comparison for Series 93×62×5.5-SBC

Specimen	Test results			Design comparisons		
	P_{Exp} (kN)	$M_{end,Exp}$ (kNm)	$M_{mid,Exp}$ (kNm)	$\frac{P_{Exp}}{P_{AISI}}$	$\frac{P_{Exp}}{P_{AISI,IR}}$	$\frac{P_{Exp}}{P_{AISC}}$
93×62×5.5-SBCe5	553.5	2.3	6.0	1.19	1.14	1.12
93×62×5.5-SBCe12	458.2	5.4	9.3	1.26	1.15	1.09
93×62×5.5-SBCe25	383.7	8.9	13.0	1.42	1.24	1.15
93×62×5.5-SBCe50	275.2	13.0	16.6	1.53	1.28	1.14
93×62×5.5-SBCe100	167.0	16.5	19.2	1.61	1.29	1.13
Mean				1.40	1.22	1.13
COV				0.125	0.057	0.020

Table 3 Test results and design strength comparison for Series 107×68×6.5-SBC

Specimen	Test results			Design comparisons		
	P_{Exp} (kN)	$M_{end,Exp}$ (kNm)	$M_{mid,Exp}$ (kNm)	$\frac{P_{Exp}}{P_{AISI}}$	$\frac{P_{Exp}}{P_{AISI,IR}}$	$\frac{P_{Exp}}{P_{AISC}}$
107×68×6.5-SBCe8	730.9	5.0	10.6	1.19	1.13	1.09
107×68×6.5-SBCe15	680.0	8.6	15.1	1.29	1.18	1.12
107×68×6.5-SBCe30	547.1	15.1	22.1	1.45	1.26	1.17
107×68×6.5-SBCe60	358.2	21.4	27.6	1.59	1.31	1.17
107×68×6.5-SBCe110	245.8	26.4	31.0	1.73	1.39	1.21
Mean				1.45	1.25	1.15
COV				0.150	0.084	0.041

Table 4 Test results and design strength comparison for Series 108×79×5.5-SBC

Specimen	Test results			Design comparisons		
	P_{Exp} (kN)	$M_{end,Exp}$ (kNm)	$M_{mid,Exp}$ (kNm)	$\frac{P_{Exp}}{P_{AISI}}$	$\frac{P_{Exp}}{P_{AISI,IR}}$	$\frac{P_{Exp}}{P_{AISC}}$
108×79×5.5-SBCe9	681.2	5.4	10.0	1.46	1.38	1.33
108×79×5.5-SBCe15	610.3	8.6	14.1	1.59	1.45	1.38
108×79×5.5-SBCe30	495.9	13.7	18.7	1.74	1.52	1.40
108×79×5.5-SBCe60	349.5	21.0	25.8	1.95	1.62	1.45
108×79×5.5-SBCe120	217.2	26.1	30.1	2.10	1.69	1.47
108×79×5.5-SBCe120#	202.5	24.4	28.3	1.97	1.58	1.38
Mean				1.80	1.54	1.40
COV				0.136	0.074	0.036

Table 5 Test results and design strength comparison for Series 125×85×6.5-SBC

Specimen	Test results			Design comparisons		
	P_{Exp} (kN)	$M_{end,Exp}$ (kNm)	$M_{mid,Exp}$ (kNm)	$\frac{P_{Exp}}{P_{AISI}}$	$\frac{P_{Exp}}{P_{AISI,IR}}$	$\frac{P_{Exp}}{P_{AISC}}$
125×85×6.5-SBCe8	983.1	6.7	18.6	1.33	1.27	1.23
125×85×6.5-SBCe15	874.7	12.1	24.1	1.44	1.32	1.26
125×85×6.5-SBCe30	713.3	22.2	33.1	1.63	1.43	1.32
125×85×6.5-SBCe60	484.8	28.1	35.5	1.64	1.38	1.24
125×85×6.5-SBCe90	389.4	34.5	40.4	1.80	1.48	1.30
Mean				1.57	1.38	1.27
COV				0.118	0.061	0.031

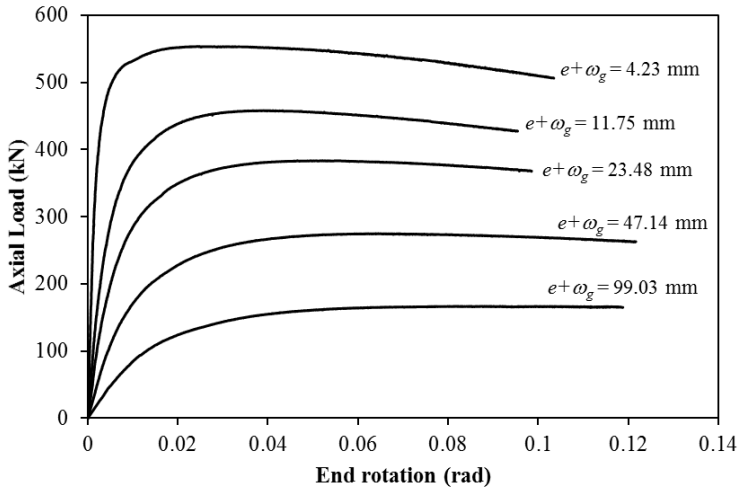

Fig. 4 Load-end rotation responses for Series 93×62×5.5-SBC

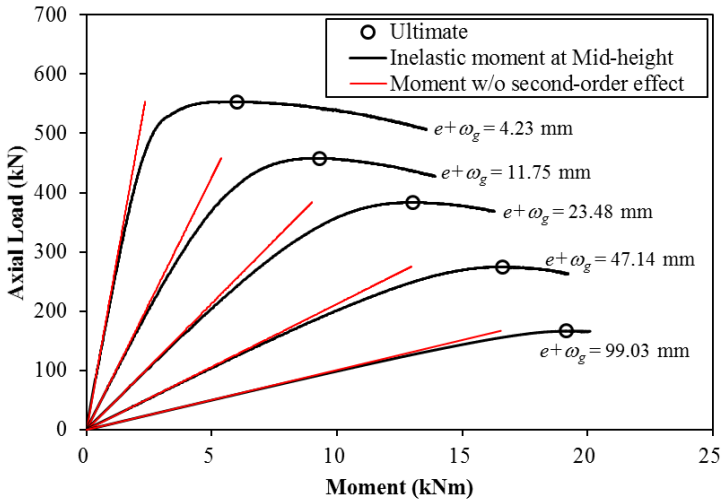

Fig. 5 Load-moment relationships for Series 93×62×5.5-SBC

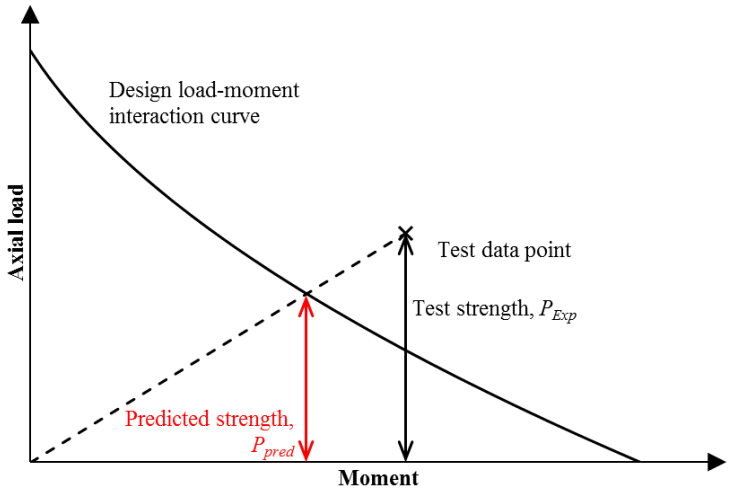

Fig. 6 Illustration of the test and predicted strengths comparison on load-moment interaction curve

5. DESIGN COMPARISONS

5.1 General

Although the design of cold-formed steel semi-oval sections is not explicitly included in the current design specifications, the experimental results were compared with the nominal strengths (unfactored design strengths) calculated by the North American Specification (AISI-S100 2016) and the American Specification (ANSI/AISC360 2016) using the interaction curves specified in these design specifications. The material properties at the location with the lowest 0.2% proof stress

were used in the nominal strength calculation for conservative predictions. The average measured cross-section dimensions as detailed in Tables 2-5 were used to predict the nominal strengths. The design strength prediction for beam-column specimen involves the calculation of bending and compressive resistances as well as the load-moment interaction relationship. The test-to-predicted strength ratio of specimen was evaluated through comparing the test strengths with the corresponding design strengths at the same initial loading eccentricity as shown in Fig. 6.

5.2 North American Specification

The beam-column interaction equation in the North American Specification (AISI-S100 2016) is shown in Eq. (6). For flexural strength calculation, two design approaches with and without considering the inelastic reserve capacity are detailed in the AISI-S100 (2016).

$$\frac{P_u}{P_n}+\frac{M_u}{M_n}\le 1 \tag{6}$$

where P_u is the design axial load, M_u is the design second-order inelastic moment as expressed by Eq. (7), P_n and M_n are the nominal flexural and compressive strengths of the SOHS calculated in accordance with the design rules for beam and column in the specification, $M_{end,u}$ is the end moment at ultimate, P_{cre} is the critical elastic buckling load of member.

$$M_u=\frac{1}{1-\dfrac{P_u}{P_{cre}}}M_{end,u} \tag{7}$$

For the approaches with and without considering the inelastic reserve capacity in flexural strength calculation, the mean values of test-to-predicted strength ratio of beam-column members are 1.36 (for $P_{Exp}/P_{AISI,IR}$) and 1.57 (for P_{Exp}/P_{AISI}), respectively, as shown in Table 6. The corresponding COV are 0.117 and 0.162, respectively. Both of the two approaches in the AISI-S100 (2016) provide quite conservative and scattered design strength predictions for SOHS short beam-columns in this study.

5.3 American Specification

The American Specification ANSI/AISC360 (2016) adopts a two-phase load-moment interaction relationship as shown in Eq. (8).

$$\begin{cases} \dfrac{P_u}{P_n}+\dfrac{8}{9}\dfrac{M_u}{M_n}\le 1 & \text{for } \dfrac{P_u}{P_n}\ge 0.2 \\ \dfrac{P_u}{2P_n}+\dfrac{M_u}{M_n}\le 1 & \text{for } \dfrac{P_u}{P_n}< 0.2 \end{cases} \tag{8}$$

The experimental results were compared with the design predictions by the American Specification (P_{AISC}) as shown in Tables 2-6. The mean value of test-to-predicted strength ratio (P_{Exp}/P_{AISC}) for all beam-columns in this study is 1.25 with the corresponding COV of 0.097. It is found from the results as shown in Table 6 that the ANSI/AISC360 (2016) provides the least conservative and the least scattered strength predictions for cold-formed steel compact SOHS subjected to combined compression and bending.

Table 6 Summary of design strength comparisons

Number of tests: 21		$\frac{P_{Exp}}{P_{AISI}}$	$\frac{P_{Exp}}{P_{AISI,IR}}$	$\frac{P_{Exp}}{P_{AISC}}$
	Mean	1.57	1.36	1.25
	COV	0.162	0.117	0.097

6. CONCLUSIONS

Experimental investigation on cold-formed steel semi-oval hollow section short members under combined compression and uniaxial bending has been conducted. A total of 21 semi-oval hollow section short beam-columns were tested at various loading eccentricities. The ultimate load-carrying capacities, the load-end rotation responses and the load-moment interaction relationship have been reported. The experimental results were compared with the design predictions by the North American Specification (AISI-S100 2016) and the American Specification (ANSI/AISC360 2016) using the interaction curves specified in these design specifications. Generally, the predictions by the North American and American Specifications are quite conservative and scattered for cold-formed steel compact semi-oval hollow section short beam-columns under combined compression and uniaxial bending.

REFERENCES

AISI-S100 2016. North American Specification for the design of cold-formed steel structural members. *AISI S100-16.* Washington,D.C., USA: American Iron and Steel Institute.

ANSI/AISC360 2016. Specification for Structural Steel Buildings. *ANSI/AISC 360-16.* Chicago, IL, USA: American Institute of Steel Construction.

Chen, J., Chan, T.M., Su, R.K.L. and Castro, J.M. (2019), “Experimental assessment of the cyclic behaviour of concrete-filled steel tubular beam-columns with octagonal sections”, *Engineering Structures*, **180**, 544-560.

Chen, M.T. and Young, B. (2018a), “Cross-sectional behavior of cold-formed steel semi-oval hollow sections”, *Engineering Structures*, **177**, 318-330.

Chen, M.T. and Young, B. (2018b), “Experimental and numerical investigation on pin-ended cold-formed steel semi-oval hollow section compression members”, *Journal of Constructional Steel Research*, **151**, 174-184.

Chen, M.T. and Young, B. (2019a), "Behavior of cold-formed steel elliptical hollow sections subjected to bending", *Journal of Constructional Steel Research*, **158**, 317-330.

Chen, M.T. and Young, B. (2019b), "Material properties and structural behavior of cold-formed steel elliptical hollow section stub columns", *Thin-Walled Structures*, **134**, 111-126.

Chen, M.T. and Young, B. (2019c), "Structural behavior of cold-formed steel semi-oval hollow section beams", *Engineering Structures*, **185**, 400-411.

Chen, M.T. and Young, B. (2019d), "Structural performance of cold-formed steel elliptical hollow section pin-ended columns", *Thin-Walled Structures*, **136**, 267-279.

Ding, F.X., Li, Z., Cheng, S. and Yu, Z.W. (2016), "Composite action of octagonal concrete-filled steel tubular stub columns under axial loading", *Thin-Walled Structures*, **107**, 453-461.

Fang, H., Chan, T.M. and Young, B. (2018), "Material properties and residual stresses of octagonal high strength steel hollow sections", *Journal of Constructional Steel Research*, **148**, 479-490.

Xu, W., Han, L.H. and Li, W. (2016a), "Performance of hexagonal CFST members under axial compression and bending", *Journal of Constructional Steel Research*, **123**, 162-175.

Xu, W., Han, L.H. and Li, W. (2016b), "Seismic performance of concrete-encased column base for hexagonal concrete-filled steel tube: experimental study", *Journal of Constructional Steel Research*, **121**, 352-369.

Zhu, J.Y., Chan, T.M. and Young, B. (2019), "Cross-sectional capacity of octagonal tubular steel stub columns under uniaxial compression", *Engineering Structures*, **184**, 480-494.